Electronic Supplementary Material (ESI) for Nanoscale.

Supporting Information

Electrostatic Assembly of a Multicomponent Peptide/Amphiphile Nanotube.

*Jenae J. Linville,[†] McKensie L. Mason,[†] Edgar U. Lopez-Torres and Jon R. Parquette[†]**

[†]Department of Chemistry, The Ohio State University, 100 W. 18th Ave. Columbus, Ohio 43210

Email: parquette.1@osu.edu

Table of Contents

Synthetic Methods and Experimental Section	S3-S7
Synthesis of Lys(NDI)-NH_2 (**2**)	S5
Zeta potential measurements	S7
TEM images and CD spectra as function of concentration, pH and **1**:**2** ratio	S7-S9
Histograms of nanostructure dimensions of $\mathbf{1}_{NT}$ and $\mathbf{2}_{NT/NR}$	S9
TEM images and CD spectra of co-assembled samples with added NaCl	S9
Comparison of the CD spectra of $\mathbf{1}_{NT}$, $\mathbf{2}_{NT/NR}$ and $\mathbf{1\text{-}2}_{NT}$	S11
CD spectra with HT voltage of $\mathbf{1\text{-}2}_{NT}$	S12
Cryo-TEM images of $\mathbf{1\text{-}2}_{NT}$	S12
FT-IR spectra of $\mathbf{1}_{NT}$, $\mathbf{2}_{NT/NR}$ and $\mathbf{1\text{-}2}_{NT}$	S13
UV and fluorescence spectra of $\mathbf{1}_{NT}$, $\mathbf{2}_{NT/NR}$ and $\mathbf{1\text{-}2}_{NT}$	S14
FRET efficiency estimation.	S15
SIM images of $\mathbf{2}_{NT/NR}$, $\mathbf{1}_{NT}$, and $\mathbf{1\text{-}2}_{NT}$, without added dye	S16
Confocal images of $\mathbf{1}_{NT}$, $\mathbf{2}_{NT/NR}$ and $\mathbf{1\text{-}2}_{NT}$	S16
pH Dependent CD and UV Spectra of $\mathbf{1\text{-}2}_{NT}$	S17
Confocal and TEM images of $\mathbf{1\text{-}2}_{NT\ a}$fter pH induced dissociation of **1**.	S17-S19
Time-dependent AFM, CD, and UV spectra .	S19-20
References	S20

Synthetic Methods and Experimental Section.

General Methods. Fluorescence microscopy experiments were performed on a Nikon A1R Live Cell Confocal microscope equipped with 32-channel PMT spectral detector. Transmission Electron Microscopy (TEM) was conducted with Technai G2 Spirit instrument running at 80.0 kV. Scanning Electron Microscopy (SEM) was carried out using an Apreo II (FEI Apreo LoVac High Resolution) instrument at 1.01 kV, 13.0 pA, and a working distance of 3-4 mm. Atomic force microscopy (AFM) was conducted in ScanAsyst mode on a Bruker AXS Dimension Icon Atomic Force Microscope and processed with Bruker nanoscope software. Infrared spectroscopy was performed in D_2O using a Shimadzu IR Affinity-1 Fourier Transform Infrared Spectrometer with CaF_2 plates. Fluorescence excitation and emission experiments were performed on a Shimadzu RF-5301PC Spectrofluorophotometer in a Spectrosil Far UV Quartz triangle cuvette. Circular dichroism (CD) measurements were run with a JASCO J-815 CD Spectrometer in a 3 mm path length quartz cuvette at 23°C unless otherwise specified. All UV measurements were conducted using Shimadzu UV-2450 spectrophotometer in a 3 mm path length quartz cuvette at 23°C unless otherwise noted. The pH measurements were obtained using a Mettler Toledo MP 125 pH meter with an InLab Micro pH probe. ESI mass spectra were recorded on a Bruker MicrOTOF coupled with HPLC. Zeta potentials were measured on Malvern Zetasizer NanoZS system with irradiation from a 632.8 nm He-Ne laser. Nikon A1R Live Cell Confocal instrument was used for confocal experiments. ^{1}H and ^{13}C NMR were recorded either at 400 MHz or 600MHz on a Bruker Avance III instrument.

Structured Illumination Microscopy (SIM): A Nikon Structured Illumination Microscopy (SIM) and STochastic Optical Reconstruction Microscopy (STORM) super-resolution system was used for SIM experiments. The fluorescence images of the assemblies were recorded the Nikon Eclipse Ti2 inverted microscope in SIM mode with excitation via three laser channels: 405 nm, 488 and 561 nm. All images were collected with a 100x oil immersion objective and processed using NIS-Elements analysis software and FIJI imaging software. The channels were merged to demonstrate colocalization of **1** and **2** within **1-2**$_{\mathbf{NT}}$.

Confocal Microscopy. Samples were deposited in aqueous solution onto 1.0 mm glass microscope slides with #1.5 glass cover slips, sealed on the edges with clear liquid nail polish. Imaging was performed using a Nikon A1R Live Cell Confocal microscope equipped with 32-channel PMT spectral detector. Samples were excited with either 402 nm, as indicated per experiment, with emission wavelengths specified or collected in spectral detector mode with separation into 32 channels with a resolution of 6 nm. Images were collected with a 100x oil immersion objective and processed using NIS- Elements analysis software and FIJI imaging software.

Transmission Electron Microscopy (TEM): Samples were dropped on carbon-coated copper grids (Ted Pella, Inc.) for 2 min. After removal of excess solution, the sample grid was negatively stained with 2% (w/w) uranyl acetate solution for 1 min. The dried specimen was observed with Technai G2 Spirit TEM instrument operating at 80 keV. Images were analyzed with either FIJI or ImageJ imaging software.

AFM: AFM images were collected on the Bruker AXS Dimension Icon Atomic Force Microscope in ScanAsyst mode using Bruker AFM silicon tips with a nitride lever under a nitrogen atmosphere in. The sample being analyzed was dropped on a freshly cleaved mica surface and dried before imaging with a resolution of 512 x 512 pixels. AFM images were analyzed with Bruker NanoScope

Analysis software. **1** was adjusted to pH > 9 then back to pH 4 and aged 24 h to ensure nanotube morphology. The co-assembly method using **1** and **2** was employed as previously described at 2 mM (overall concentration) and aged 3 days before being dropped on a freshly cleaved mica surface.

Steady State Fluorescence: Stock solutions of each experiment were measured at indicated time scales and concentrations. The triangle cuvette was used to ensure no inner filter effect while gaining insight into the fluorescence at appropriate concentrations. Monomer $\mathbf{2_M}$, was excited at 330 nm and **1** was excited at 420 nm. Both components were exited at 405 nm to confirm the viability of both confocal and SIM imaging methods.

Synthetic Methods. The syntheses of EFEK(DAC)-NH_2 (**1**) and Lys(NDI)-NH_2 (**2**) were adapted from previously published methods.[1,2]

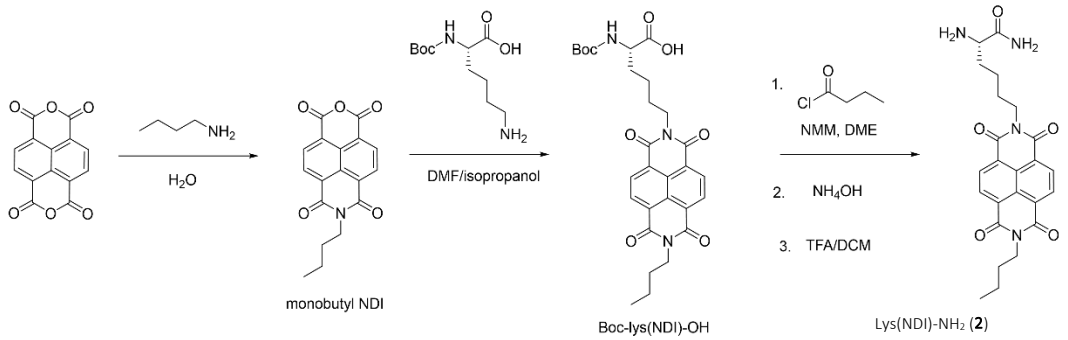

Scheme 1. Synthesis of Lys(NDI)-NH_2 (**2**), adapted from ref. 1.

Lys(NDI)-NH_2 (2). (i) Naphthalenetetracarboxylic dianhydride (NDA, 10 g, 37.29 mmol, 1 eq.) was treated with aq. sodium hydroxide (1M, 137 mL). The mixture was heated to 65°C for 1.5 h until all solids dissolved. After cooling to room temperature, the solution was adjusted to ~pH 6-7 with 1 M aq. H_3PO_4. *n*-Butylamine (3.66 mL, 37.03 mmol, 1 eq.) was introduced and the solution was heated to 125°C for 19 h. The mixture was cooled to ambient temperature and acetic acid (5 mL) was added to the orange solution, which was filtered to obtain a cream-colored precipitate.

The solid was further dried by lyophilization affording a cream-colored solid (5.74 g, 47.8%, monobutyl NDI). The product was used directly in the following step. ^{1}H NMR (400 MHz, DMSO-d6) δ 8.52 (2H, d, *J* = 7.5 Hz), 8.10 (2H, d, *J* = 7.5 Hz), 4.05 (2H, t, *J* = 14.7 Hz), 1.63 (2H, m), 1.36 (2H, m), 0.93 (3H, t, *J* = 7.3 Hz).

(ii) ***N*-Boc-L-lys-OH.** N_α-(*tert*-butoxycarbonyl)-L-lysine (N_α-Boc-L-lysine) (4.37 g, 17.75 mmol, 1 eq.) was added to the monobutyl NDI intermediate produced in the previous step (5.74 g, 17.75 mmol, 1 eq.) in 100 mL isopropanol/DMF (1:2) then stirred at 50°C under nitrogen atmosphere for 3 h until dissolved. After heating the solution to 125°C for 19 h, the solvent was removed under reduced pressure and the crude product was purified by flash column chromatography affording a yellow solid, Boc-lys(NDI)-OH (eluent gradient:100% CH_2Cl_2 to 1:2 CH_2Cl_2:CH_3OH). ^{1}H NMR (400 MHz, $CDCl_3$) δ 8.74 (4H, s), 5.21 (1H, s), 4.31 (1H, s), 4.21 (4H, m), 1.97 (1H, s), 1.71-1.85 (5H, m), 1.44-1.69 (13H, m), 0.99 (3H, t, *J* = 7.3).

(iii) Ethyl chloroformate (40 µL, 0.42 mmol, 1.2 eq.) and *N*-methylmorpholine (NMM, 0.5 mL, 4.55 mmol, 12.6 eq.) was added to N_α-Boc-L-lys-OH (200 mg, 0.36 mmol, 1 eq.) in dimethoxyethane (DME, 2 mL) at 0°C. The mixture was stirred at 0°C for 1 h under nitrogen atmosphere, then NH_4OH (0.5 mL, 18.32 mmol, 50.9 eq.) was added and stirred for 16 h at rt. The solution was treated with aq. 1M $NaHSO_4$ extracted with ethyl acetate. The organic solution was then washed with water, 4% aq, $NaHCO_3$ and brine. Evaporation of the organic layer provided a white solid. The white solid as treated with a mixture of trifluoracetic acid and triethylsilane (6 mL, 95/5 v/v) and stirred at rt for 1 h. The solvent was then evaporated under reduced pressure to afford a yellow/tan solid. The solid was dispersed in CH_2Cl_2 and the mixture was centrifuged to obtain a yellow/tan pellet. Additionally the supernatant was concentrated under reduced pressure and treated with diethyl ether to form a tan precipitate, which was separated by centrifugation. The

tan solids were combined and further purified via reversed-phased HPLC on preparative Waters XBridge C8 column eluting with a gradient of CH_3CN/water containing 0.1 % TFA (30%-100% CH_3CN over 45 min) and dried via lyophilization to get a white powder (31.8 mg, 19.6%). ^1H NMR (400 MHz, DMSO-d6) δ 8.59 (4H, d), 7.97 (2H, s), 7.76 (1H, s), 7.49 (1H, s), 4.00 (4H, t, *J* = 14.8 Hz), 3.65 (1H, s), 1.67-1.74 (2H, m), 1.54-1.64 (4H, m), 1.29-1.39 (4H, m), 0.88 (3H, t, *J* = 14.8 Hz)

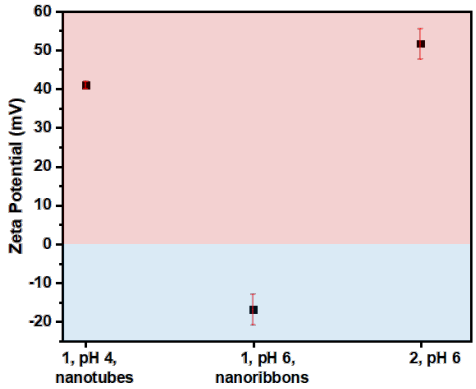

Figure S1. Zeta potential measurements. Left: nanotubes of **1**, 1 mM, aged for 24 h at pH 4.0. Middle: nanoribbons of **1**, 1 mM, aged for 24 h at pH 6.5. Right: nanoribbons/nanotubes of **2**, 1 mM, aged for 24 h. at pH 6.5.

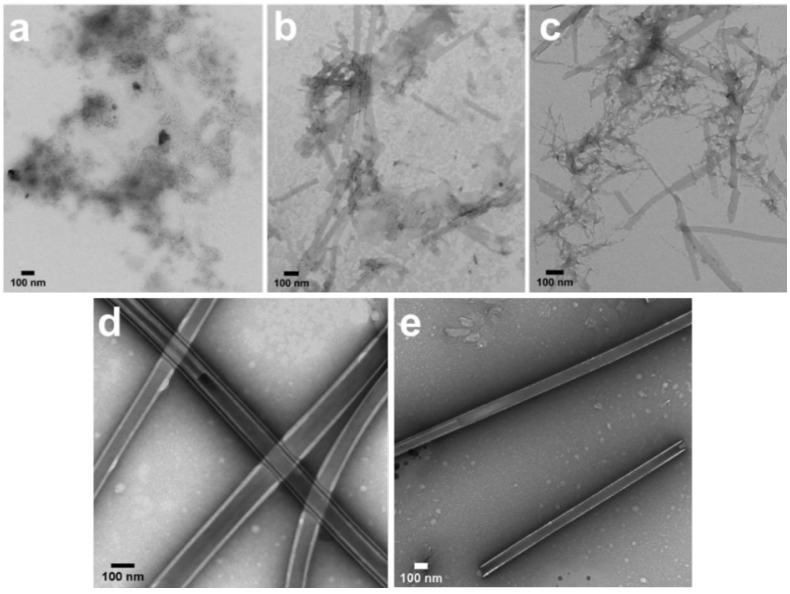

Figure S2. Concentration dependence of the co-assembly of **1-2**$_{NT}$. Components **1**$_{NT}$ and **2**$_M$ (1:1) were combined in water at pH 6.0, aged for 3d at pH 6.0 at various overall concentrations :(a) 0.25 mM (b) 0.5 mM (c) 1 mM (d) 2 mM (e) 4 mM.

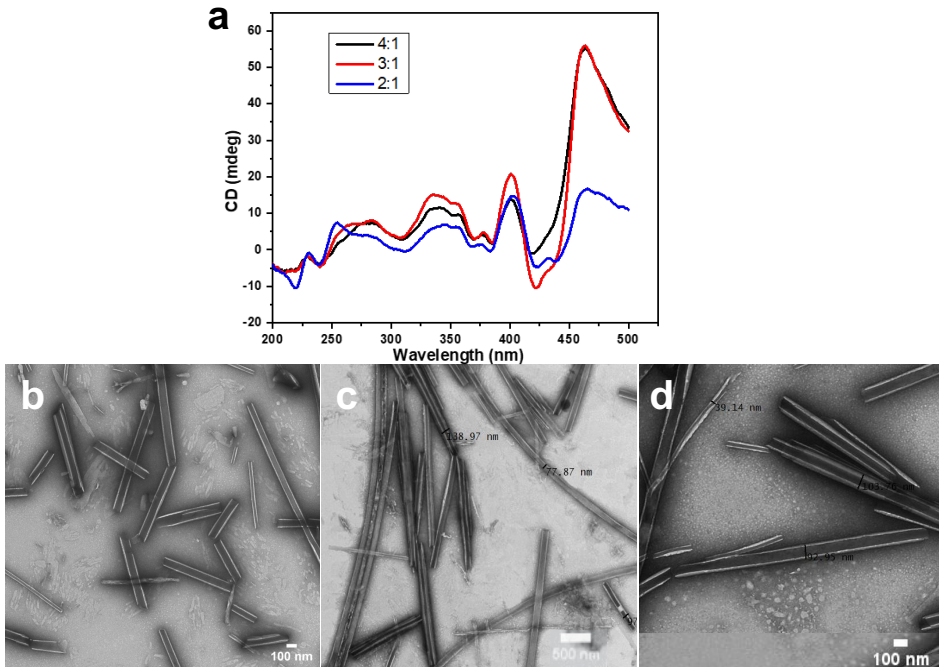

Figure S3. CD spectra and TEM images of the co-assembly of **1-2**$_{NT}$ as a function of the ratio of **1**$_{NT}$ and **2**$_{M}$, after 3d at pH 6.2 at 2 mM (total concentration). Samples formed by combining **1**$_{NT}$ with monomeric **2**$_{M}$, then immediately adjusting to pH 6.2 and aging for 3d at 2 mM (total concentration); probed at various ratios of **1**$_{NT}$ and **2**$_{M}$**.** (a) CD spectra of the **1-2**$_{NT}$ at various ratios, and corresponding TEM images at three (**2**$_{M}$:**1**$_{NT}$) ratios: (b) 2:1 (c) 3:1 and (d) 4:1.

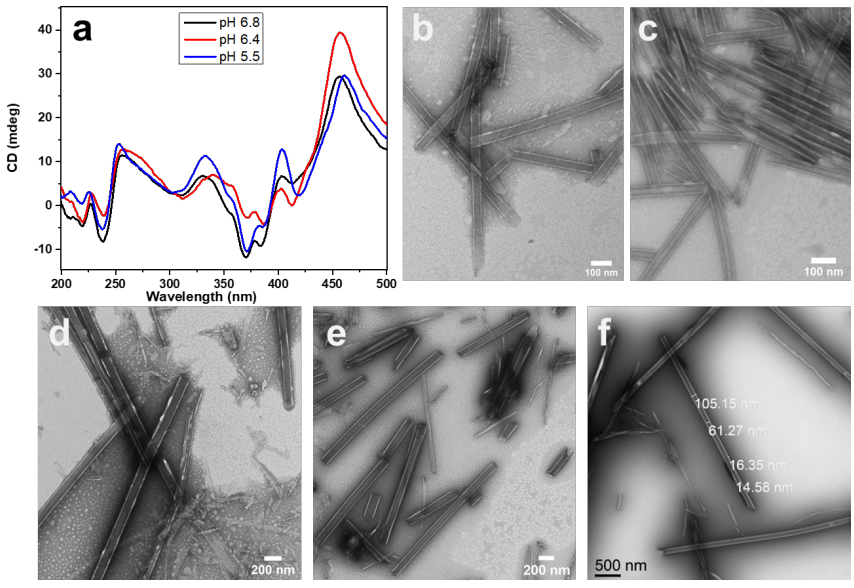

Figure S4. CD spectra and TEM images of effect of pH on the co-assembly of **1**$_{NT}$ and **2**$_{M}$ (1:1). Samples prepared using the standard conditions: **1**$_{NT}$ combined with **2**$_{M}$, then immediately adjusted to the pH indicated, and aged for 3d at 2 mM overall concentrations. TEM was used to visualize the structures while (a) pH-dependent CD spectra and TEM images at the pH values: (b) 5.1 (c) 5.2 (d) 5.5 (e) 6.4 (f) 6.8.

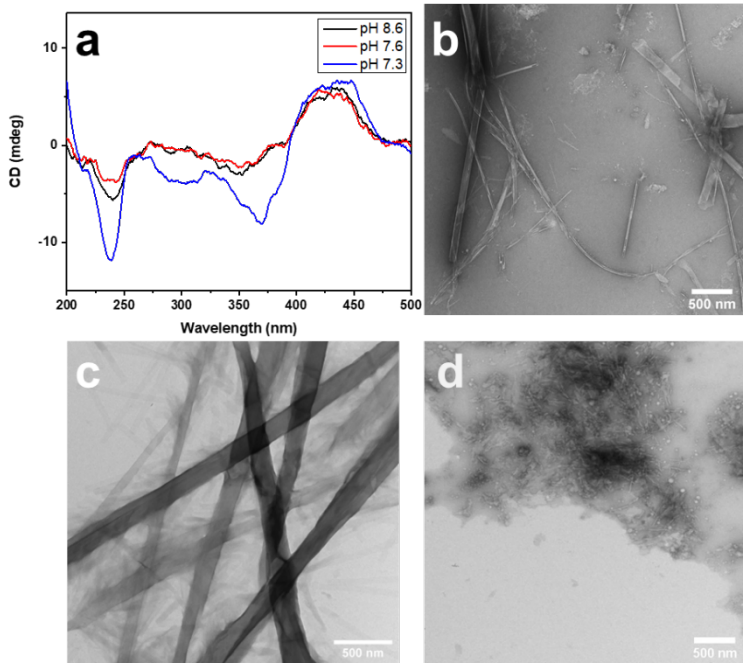

Figure S5. TEM images and CD spectra of co-assembled samples prepared at pH values that did not produce the co-assembled nanotube under standard formation conditions (combined $\mathbf{1}_{NT}$ and $\mathbf{2}_{M}$ (1:1) then immediately adjusted to the pH indicated, and aged for 3 d at 2 mM (overall concentration)). (c) CD spectra and TEM images at (b) pH 7.3 (c) pH 7.6 (d) pH 8.6.

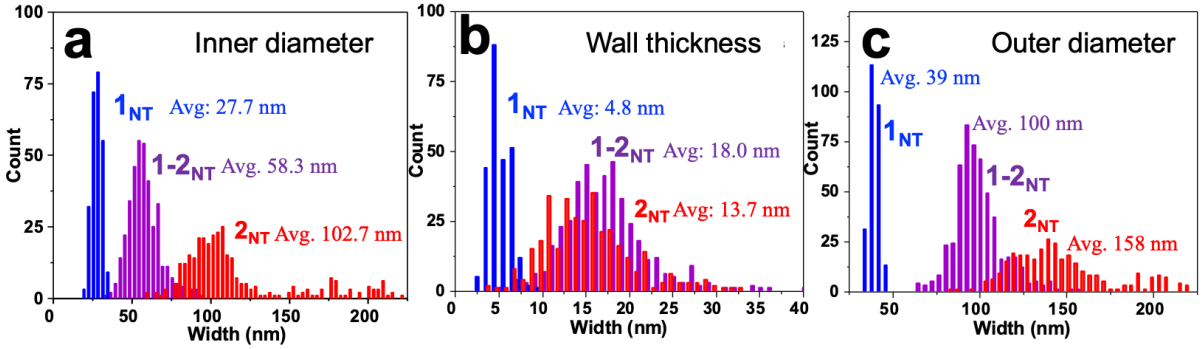

Figure S6. Measurements depicted as histograms of $\mathbf{1}_{NT}$, $\mathbf{2}_{NT}$, and the $\mathbf{1\text{-}2}_{NT}$ nanotube from aggregated data from TEM images of 300-500 nanostructures. (a) inner channel (b) wall thickness, and (c) diameter. Color coding: $\mathbf{1}_{NT}$ (blue), $\mathbf{2}_{NT}$ (red), $\mathbf{1\text{-}2}_{NT}$ (purple).

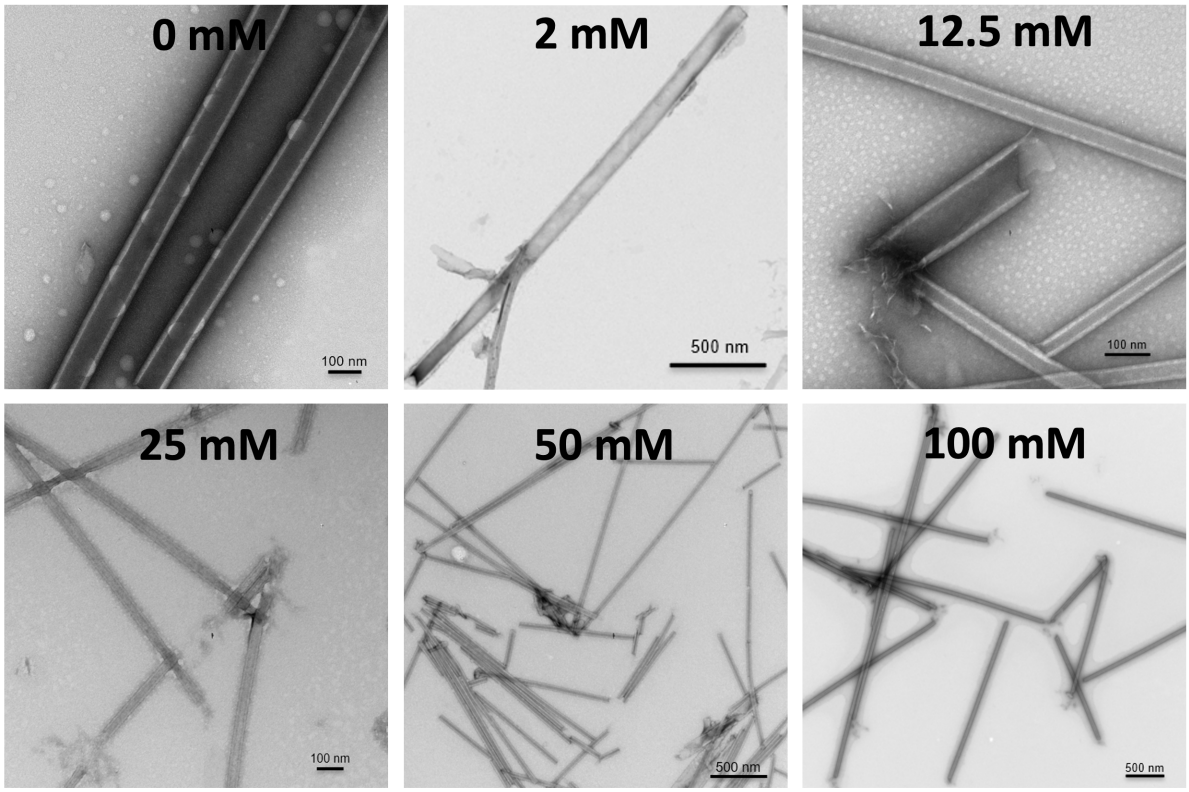

Figure S7. TEM images of samples from co-assembly experiments performed under the standard conditions with added NaCl (combined $\mathbf{1}_{NT}$ and $\mathbf{2}_{M}$ (1:1) then immediately adjusted to the pH 6.3, and aged for 3 d at 2 mM (overall concentration)).

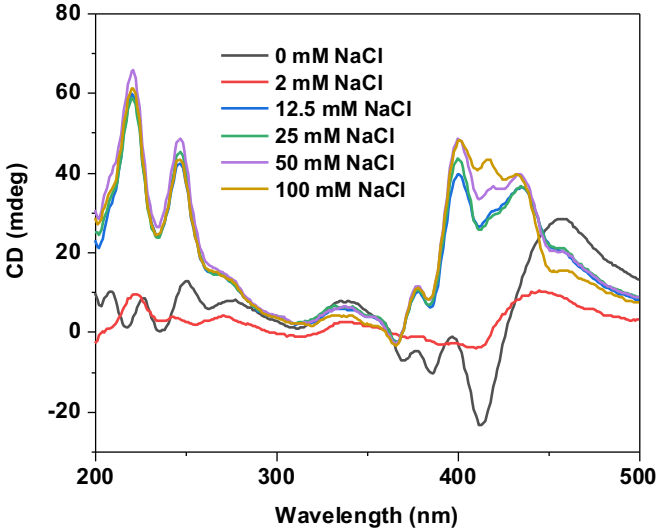

Figure S8. CD spectra of co-assembled samples with added NaCl under standard formation conditions (combined $\mathbf{1}_{NT}$ and $\mathbf{2}_{M}$ (1:1) then immediately adjusted to the pH 6.3, and aged for 3 d at 2 mM (overall concentration)).

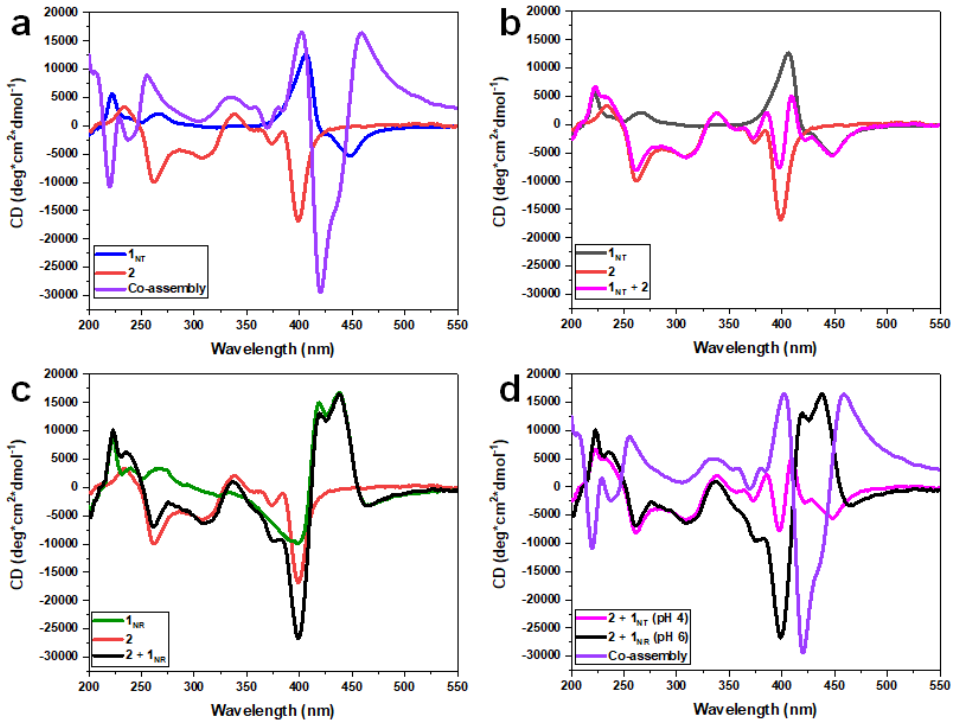

Figure S9. Comparison of the CD spectra of **1**, **2** and **1-2$_{NT}$** (a) 1 mM **1$_{NT}$** (blue) at pH 4 aged for 24 h, **2$_{NT}$** (red) aged at 1 mM for 24 h, and the co-assembled **1-2$_{NT}$**, formed by combining **1$_{NT}$** with **2$_{M}$**, then immediately adjusting to pH 6.0 ± 0.5, and aging for 3d at 2 mM (total concentration). (b) The mathematical sum of the mono-component CD spectra of **1** and **2**: summation of CD of **1$_{NT}$** (1 mM, grey) and **2$_{NT/NR}$** (1 mM, red) with the summed spectra shown in pink. (c) summation of nanoribbons **1$_{NR}$** (1 mM, green) and **2$_{NT}$** (1 mM, red), and the summed spectra of the two (black). (d) co-plot of the two calculated mathematically summed spectra from b and c, (pink and black, respectively) with the experimental spectrum of **1-2$_{NT}$** (purple).

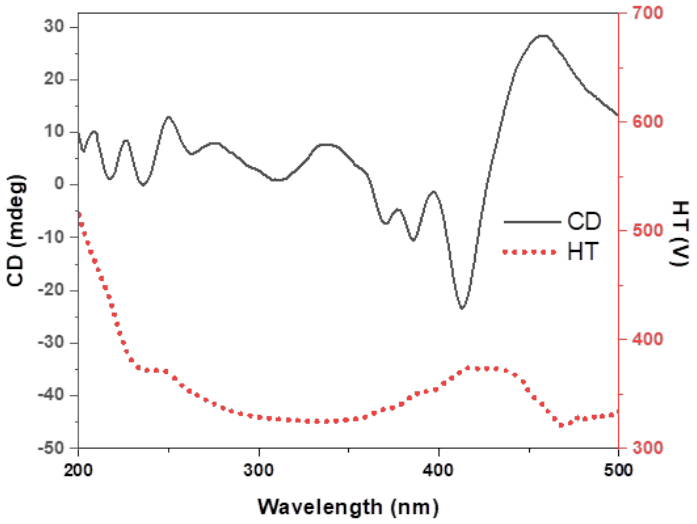

Figure S10. CD spectra with HT voltage of **1-2$_{NT}$,** assembled under the standard conditions (combined **1$_{NT}$** and **2$_{M}$** (1:1,) then immediately adjusted to the pH 6.3, and aged for 3 d at 2 mM (overall concentration)).

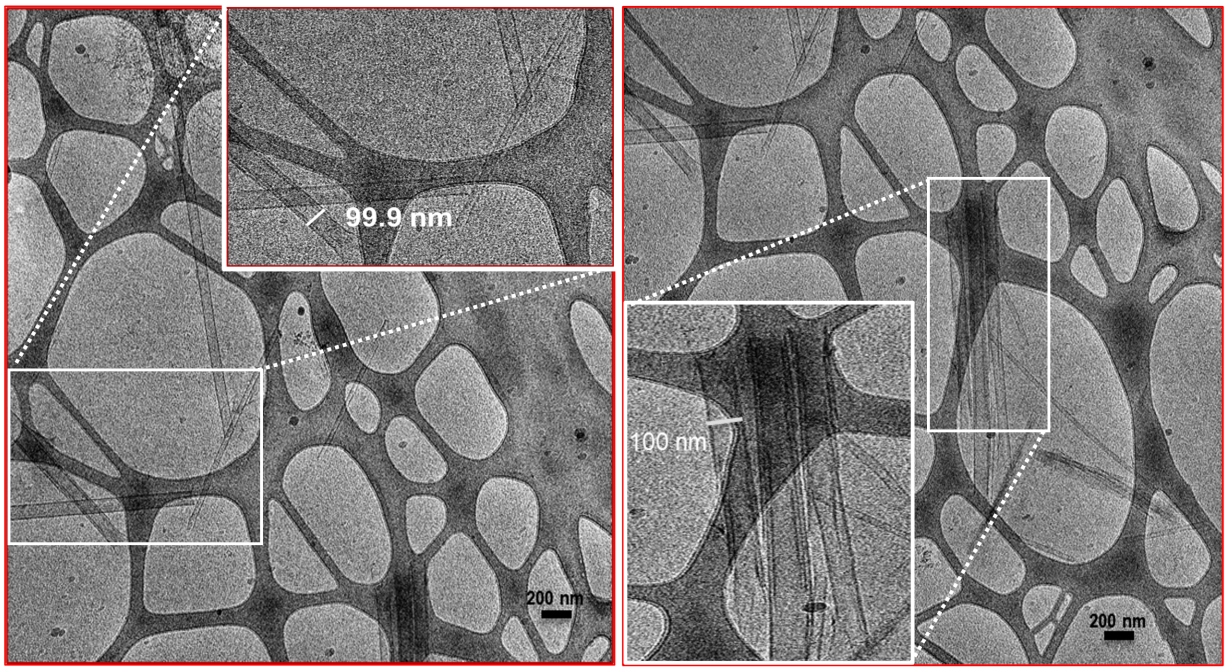

Figure S11. Cryo-TEM images of **1-2$_{NT}$.** Sample was prepared by combining **1$_{NT}$** and **2$_{M}$** (1:1, 2 mM (total), pH 6.5, 3d), then was pelleted by centrifugation (5000 rpm) and redissolved in water to increase the concentration (pH 6.5, ~8 mM). The sample was placed on lacey carbon grids, which were vitrified using an FEI Vitrobot Mark IV and imaged using the Thermo Scientific Glacios Cryo-TEM.

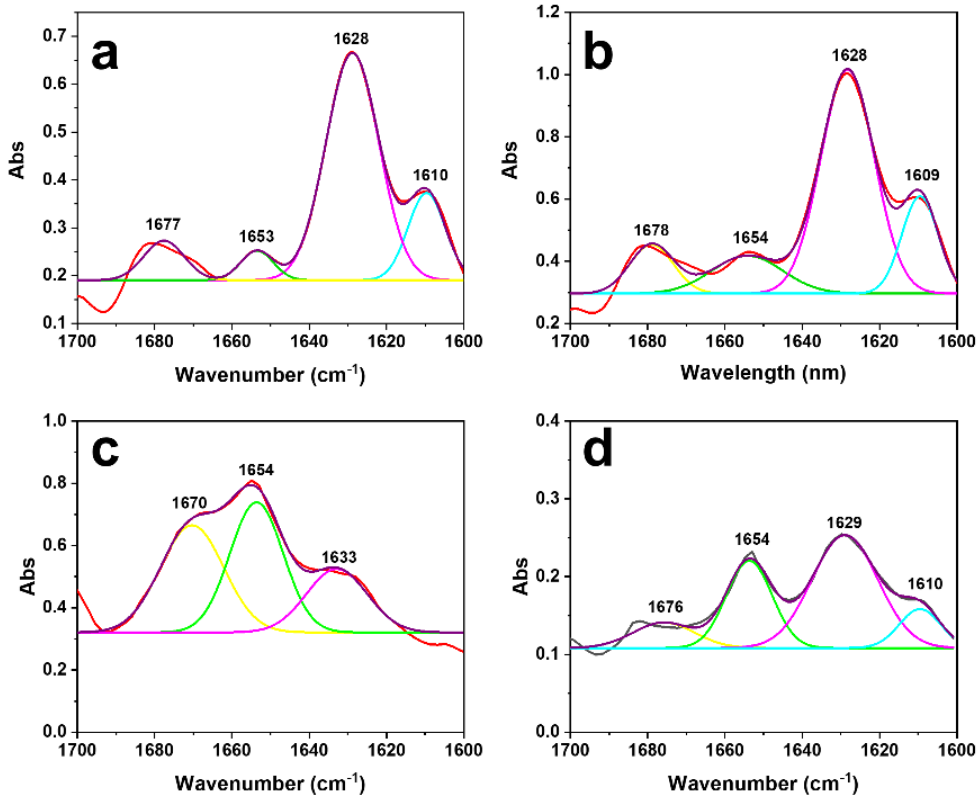

Sample	β-Sheet (%)	Random Coil (%)
EFEK(DAC), **1**, pH 4.0	85.7	14.3
EFEK(DAC), **1** , pH 6.0	79.0	21.0
NDI-Amp, **2**	18.4	81.6
Co-assembly	60.5	39.5

Figure S12. FT-IR spectra of (a) $\mathbf{1}_{\mathbf{NT}}$ (assembled at pH 4.0), (b) $\mathbf{1}_{\mathbf{NR}}$ (assembled at pH 6.0), (c) $\mathbf{2}_{\mathbf{NT/NR}}$ and (d) $\mathbf{1\text{-}2}_{\mathbf{NT}}$. Samples of **1** (a,b) were assembled in D_2O at 0.25 mM (pH 4.0) or 10 mM (pH 6.0), then pH was adjusted to 9 with 1M aq. NaOH to promote disassembly prior to adjustment to the desired pH with 1M aq. HCl or 1M aq. NaOH. Component $\mathbf{2}_{\mathbf{M}}$ (in c) was assembled at 1 mM, and $\mathbf{1\text{-}2}_{\mathbf{NT}}$ (in d) was assembled at 1 mM (each) in D_2O at pH 6.0. After 24 h, the samples were frozen in dry ice and dried by lyophilization. Solid samples were deposited on CaF_2 plates with D_2O for measurement. Measurements were subtracted from a D_2O baseline. The peak at ~1671-1678 cm^{-1} was attributed to residual trifluoroacetic acid (TFA) from HPLC purification.[3] The table provides relative percentages of β-sheet and random coil secondary structure, estimated from the integrated peaks.

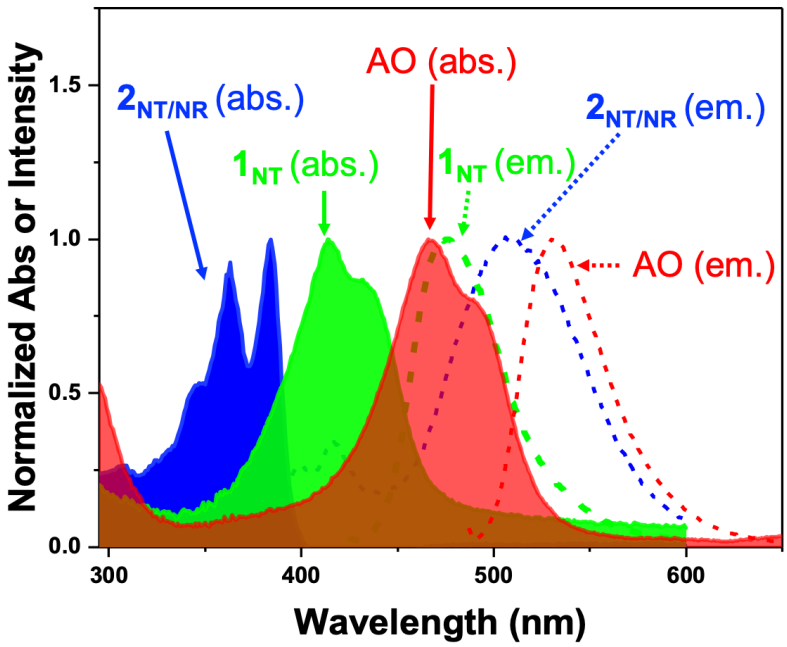

Figure S13. Normalized UV-vis and emission spectra of $\mathbf{1}_{NT}$, $\mathbf{2}_{NT/NR}$, and acridine orange shown to determine their spectral overlap and ideal excitation and emission wavelengths for imaging and FRET experiments. UV-vis spectra were acquired using a 1 mm cuvette and fluorescence spectra were acquired using a triangular quartz cuvette. Component $\mathbf{2}_{NT/NR}$ was excited at 405 nm, and $\mathbf{1}_{NT}$ was excited at 488 nm, and acridine orange was excited at 561 nm.

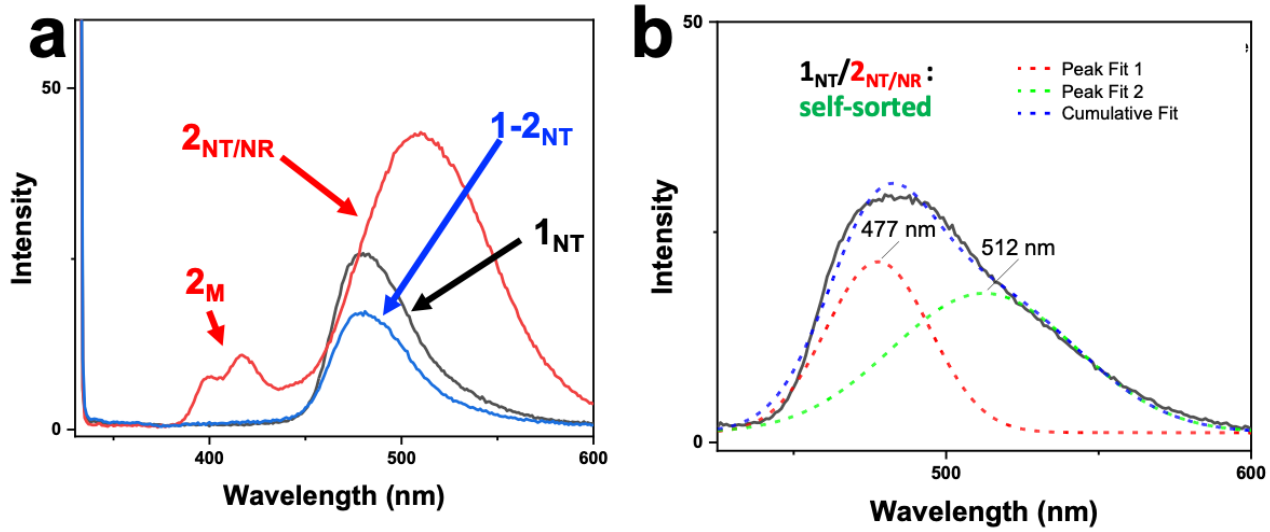

Figure S14. Emission spectra acquired in a triangular quartz cuvette with 330 nm excitation. (a) Emission of $\mathbf{1}_{NT}$ and $\mathbf{2}_{NT/NR}$, compared to a 1:1 co-assembled sample aged 3 days at pH 6.0 ($\mathbf{1}$-$\mathbf{2}_{NT}$); and (b) deconvoluted emission of a self-sorted, physical mixture of $\mathbf{1}_{NT}$ and $\mathbf{2}_{NT/NR}$ showing two peaks with maximum intensities at 477 and 512 nm.

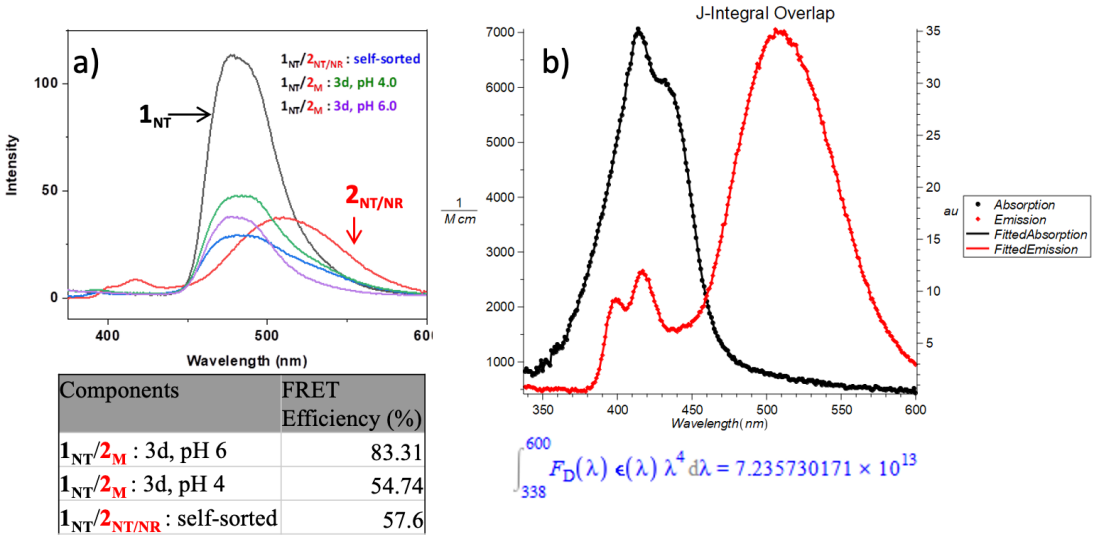

Components	FRET Efficiency (%)
$1_{NT}/2_{M}$: 3d, pH 6	83.31
$1_{NT}/2_{M}$: 3d, pH 4	54.74
$1_{NT}/2_{NT/NR}$: self-sorted	57.6

Figure S15. (a) FRET efficiency of $\mathbf{1_{NT}}$ and $\mathbf{2_{NT/NR}}$ compared with a self-sorted, mixture of preassembled $\mathbf{1_{NT}}$ and $\mathbf{2_{NT/NR}}$, a mixture of $\mathbf{1_{NT}}$ and $\mathbf{2_{M}}$, co-assembled for 3d at pH 4.0, and that same mixture adjusted to pH 6.0 prior to aging for 3d. Emission spectra acquired in a triangular quartz cuvette with 330 nm excitation. The FRET efficiency was calculated using this equation: $E = 1 - \frac{F_{DA}}{F_D}$ where E is FRET efficiency, F_D is fluorescence intensity of the donor and F_{DA} is fluorescence intensity of the donor in the presence of acceptor. As the emission of the NDI and DAC chromophores in **1** and **2** significantly overlap, the efficiencies were estimated at 560 nm to minimize the overlap. (b) Calculated overlap J-integral of the spectral overlap of the emission $\mathbf{2_{NT/NR}}$ and the absorption of $\mathbf{1_{NT}}$. Determined using code implemented in Maple software described by Harvey and Langlois.[4] J-integral 7.23 x 10^{13} ($M^{-1}cm^{-1}nm^4$); Average deviation of calculated fits from measured data was (Em.) 1.51 x 10^{-15} and (Abs.)-3.35 x 10^{-14}.

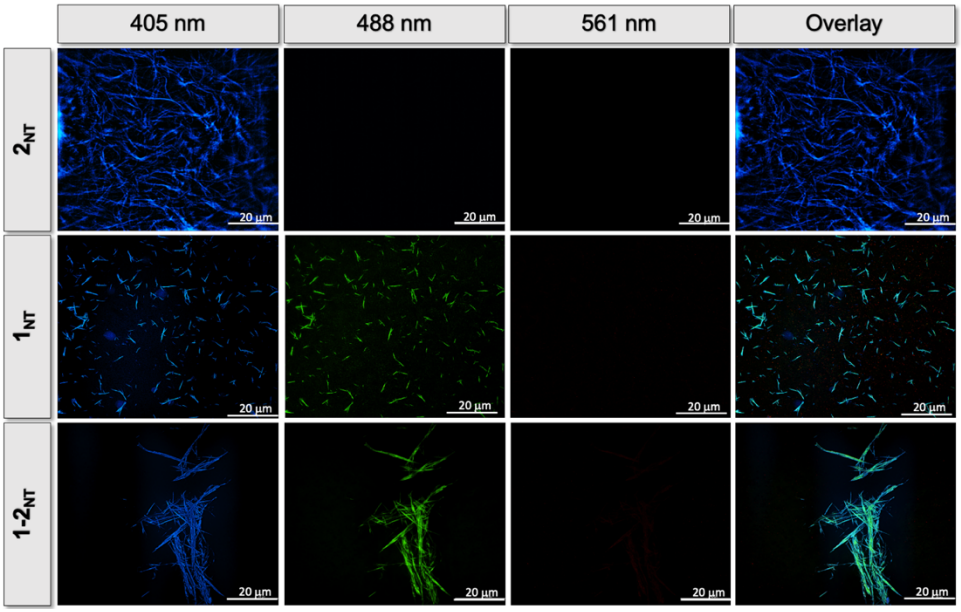

Fig. S16. SIM images of $\mathbf{2}_{\mathbf{NT/NR}}$ (1 mM, pH 6.5, top), $\mathbf{1}_{\mathbf{NT}}$ (1 mM, pH 6.5, middle), and $\mathbf{1\text{-}2}_{\mathbf{NT}}$ (2 mM, pH 6.5, bottom), without added dye as a function of excitation laser (405 nm-blue, 488 nm-green, and 561 nm-red) and overlayed image of all excitation channels.

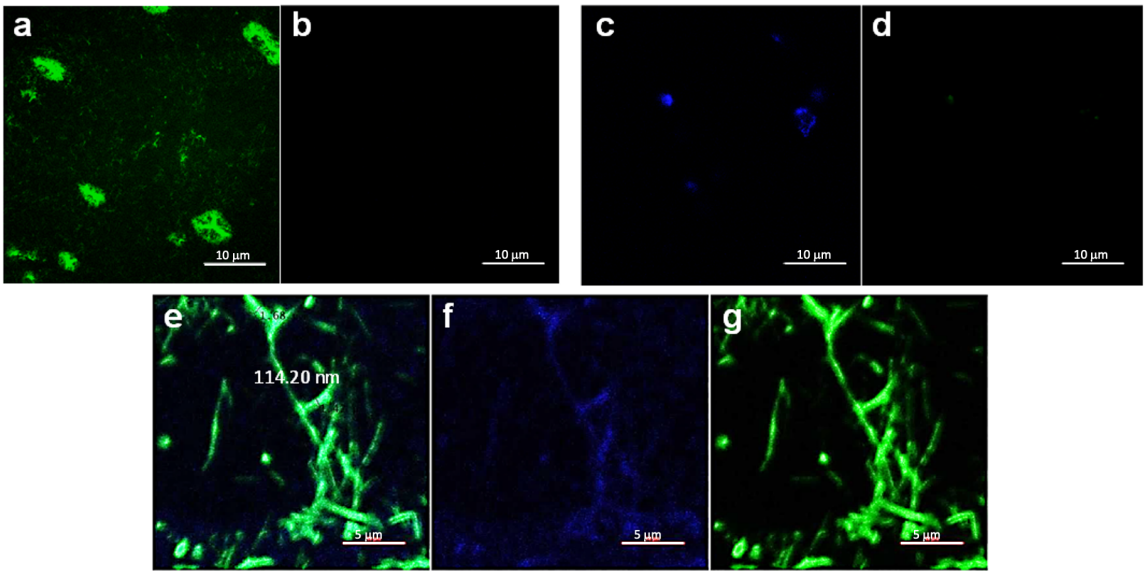

Figure S17. Confocal images of $\mathbf{1}_{\mathbf{NT}}$, $\mathbf{2}_{\mathbf{NT}}$ and $\mathbf{1\text{-}2}_{\mathbf{NT}}$ collected from emission ($\lambda_{exc.}$ 402 nm,) ranges of 400-430 nm and 580-590 nm. Images: (a) $\mathbf{1}_{\mathbf{NT}}$ from 580-590 nm, (b) $\mathbf{2}_{\mathbf{NT}}$ from 580-590 nm, (c) $\mathbf{2}_{\mathbf{NT}}$ from 400-430 nm (d) $\mathbf{1}_{\mathbf{NT}}$ from 400-430 nm, (e) Overlaid images (f) and (g), (f) $\mathbf{1\text{-}2}_{\mathbf{NT}}$ from 400-430 nm, (g) $\mathbf{1\text{-}2}_{\mathbf{NT}}$ from 580-590 nm. In (a-d) the scale bar is 10 µm and in (e-g) the scale bar is 5 µm.

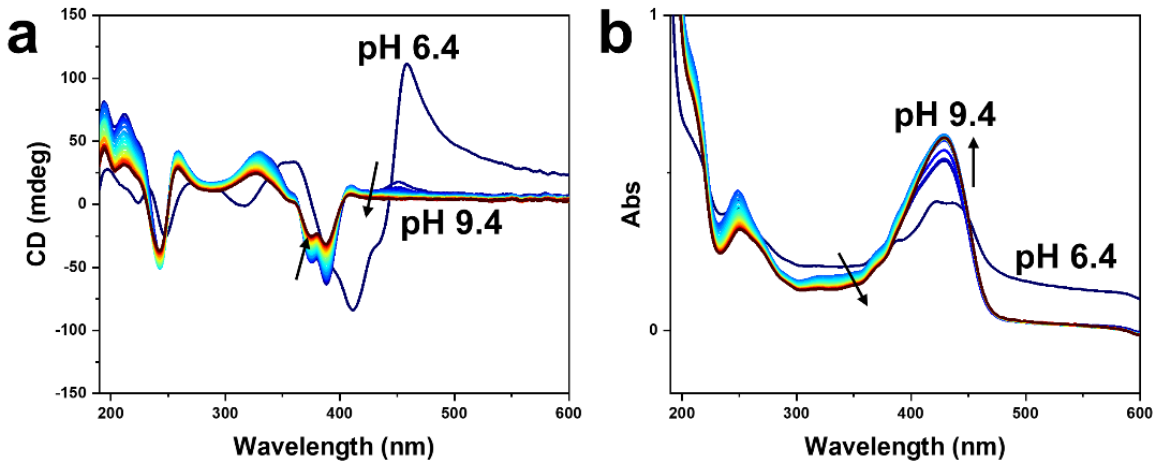

Figure S18. (a) CD and (b) UV-vis absorbance spectra of a 2 mM 1:1 co-assembled sample of $\mathbf{1}_{NT}$ and $\mathbf{2}_{M}$ aged 3 d at pH 6.4, then adjusted to pH 9.4 and monitored over 2 h, acquired in a 1 mm cuvette.

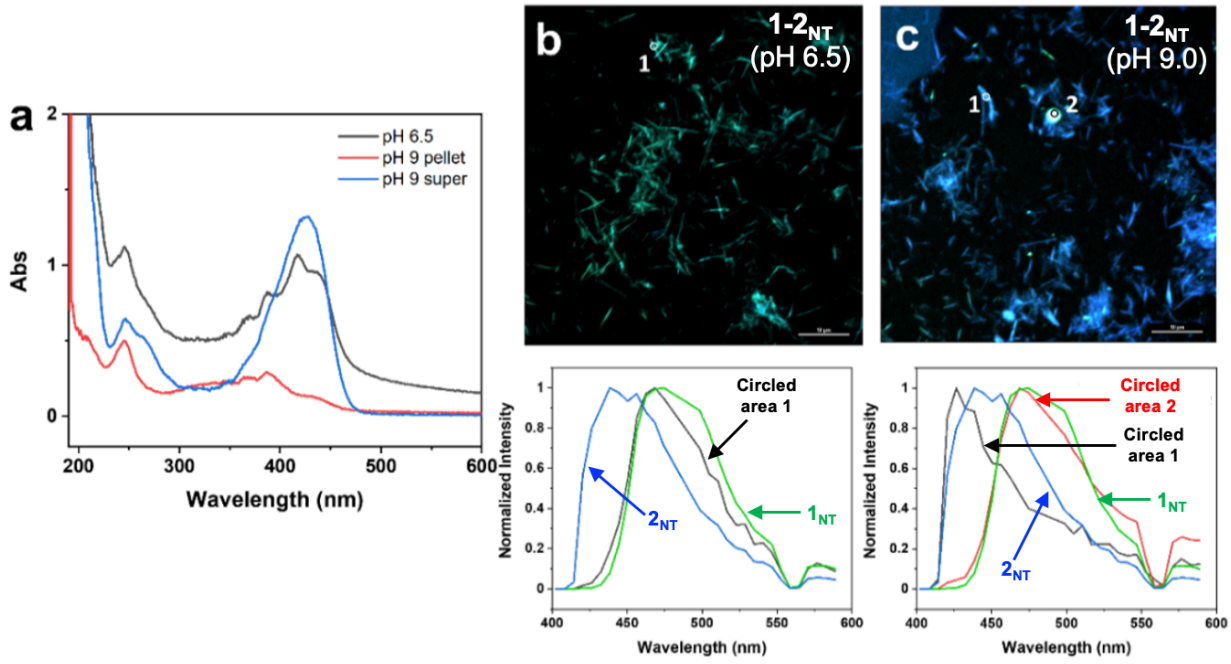

Figure S19. Dissociation of **1** from **1-2**$_{NT}$ induced at pH 9.0. **1-2**$_{NT}$ (prepared by combining $\mathbf{1}_{NT}$ and $\mathbf{2}_{M}$ (1 mM each) and aging for 3d at pH 6.5. The sample was then adjusted to pH 9.0 and immediately centrifuged at 5000 rpm for 10 min to obtain a pellet and supernatent. (a) UV-vis spectra of **1-2**$_{NT}$ at pH 6.5 and after changing pH to 9.5. Confocal fluorescence images with emission profiles of **1-2**$_{NT}$ at (b) pH 6.5 and (c) the pellet formed after pH change to pH 9.0 and centrifugation. Confocal fluorescence images were taken in spectral detector mode, by excitation at 402 nm, with 6 nm resolution and 32 channels, which were merged together. Emission profiles were generated from circled areas in the confocal images and co-plotted with emission spectra from confocal images taken of $\mathbf{1}_{NT}$ and $\mathbf{2}_{M}$ samples individually.

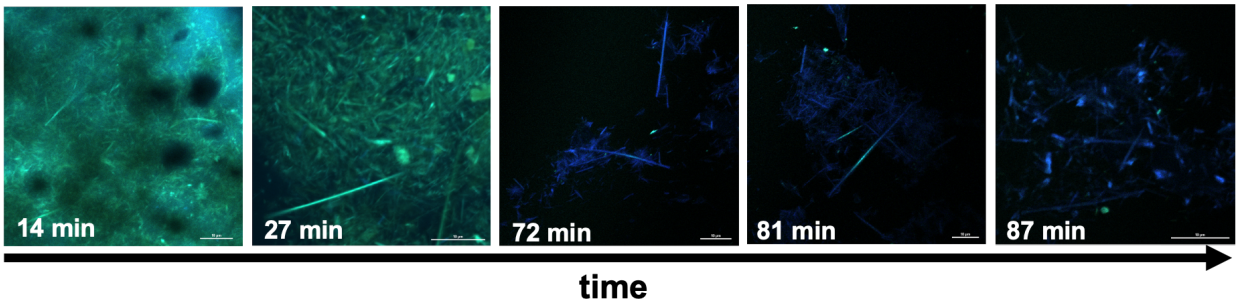

Figure S20. (a) Confocal fluorescence images of **1-2$_{NT}$** (2 mM) after 3d at pH 6.5 then adjusted to pH 9.0 and immediately placed on a glass slide for imaging over time. Selected images in show a gradual emission color change from pseudo color green (**1-2$_{NT}$**) to blue (**2$_{NT}$**) over time.

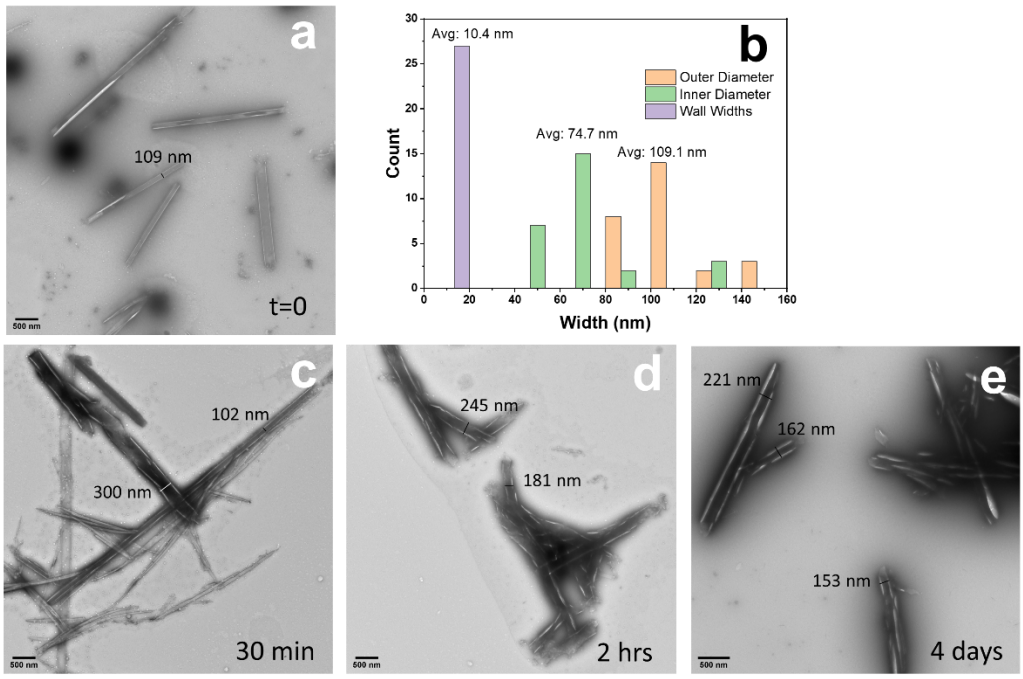

Figure S21. Representative TEM images (a, c-e) of **1-2$_{NT}$** (2 mM overall) after 3 d at pH 6.5, then adjusted to pH 9.0 and monitored over time. (b) A histogram of measurements taken from nanotubes imaged immediately after adjusting to pH 9.0 (27 measurements, generated using FIJI imaging software) showed that the average outer diameter was 109.1 nm, the inner diameter was 74.7 nm, and the wall thickness was 10.4 nm. Compared to average measurements of **1-2$_{NT}$**, the nanotubes observed immediately after adjusting to pH 9.0 displayed a slightly larger outer diameter (109.1 nm at pH 9.0 vs. 101.2 nm at pH 6.5), a larger inner diameter (74.7 nm at pH 9.0 vs 58.3 nm at pH 6.0) and smaller wall thicknesses (10.4 nm at pH 9.0 vs 16.5 nm at pH 6.0). TEM images taken of the pH 9.0 sample after (c) 30 min, (d) 2 h, and (e) 4 days revealed an increase in nanotube diameter to 150-300 nm, similar to the diameter of **2$_{NT}$**.

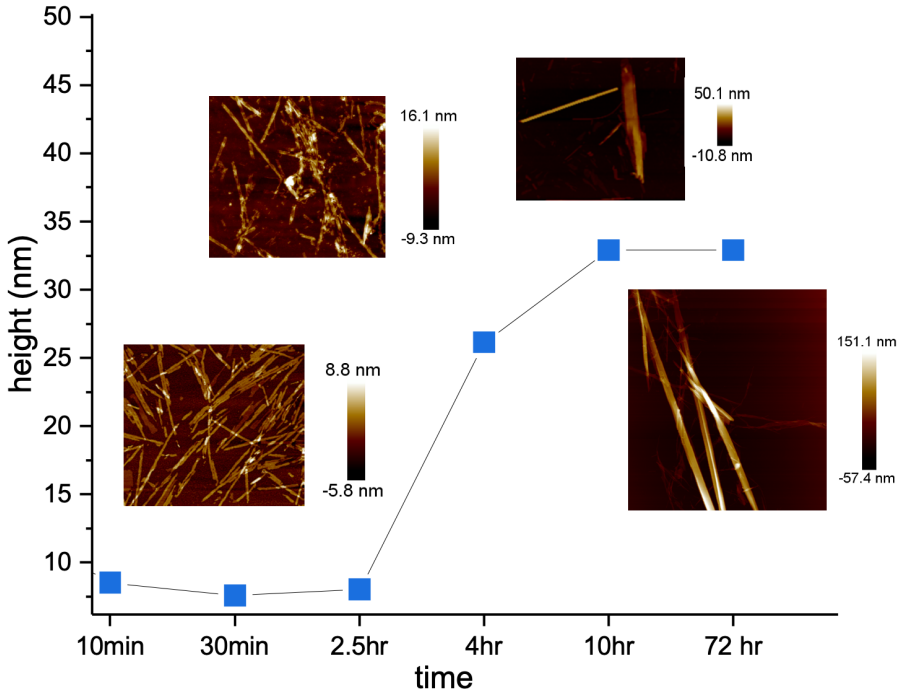

Figure S22. AFM height measurements displayed at various time points represented by the blue squares. Average cross-sectional heights based on ~150 measurements. The co-assembly sample was prepared by combining $\mathbf{1}_{NT}$ to $\mathbf{2}_{M}$ at pH 6.4 (1:1, 2 mM overall) and monitored over time. AFM images were imaged on freshly cleaved mica. One drop of the stock solution was dropped on the freshly cleaved mica and also prepared simultaneously for TEM imaging (see Fig. 5 in manuscript) at the concentration they were aged at (2 mM). The AFM sample was dried onto the mica, rinsed one time with a drop of water, dried again, and taken immediately for imaging.

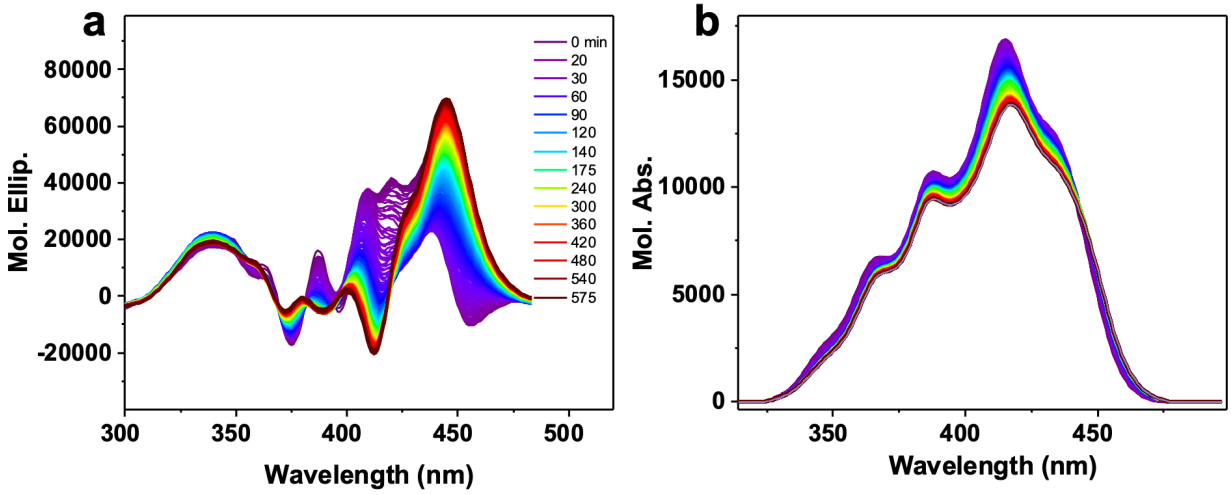

Figure S23. (a) CD and (b) UV-vis absorbance spectra of a sample of $\mathbf{1}_{NT}$ and $\mathbf{2}_{M}$ combined at pH 6.2 (2 mM, 1:1) and monitored for the first 9.5 h.

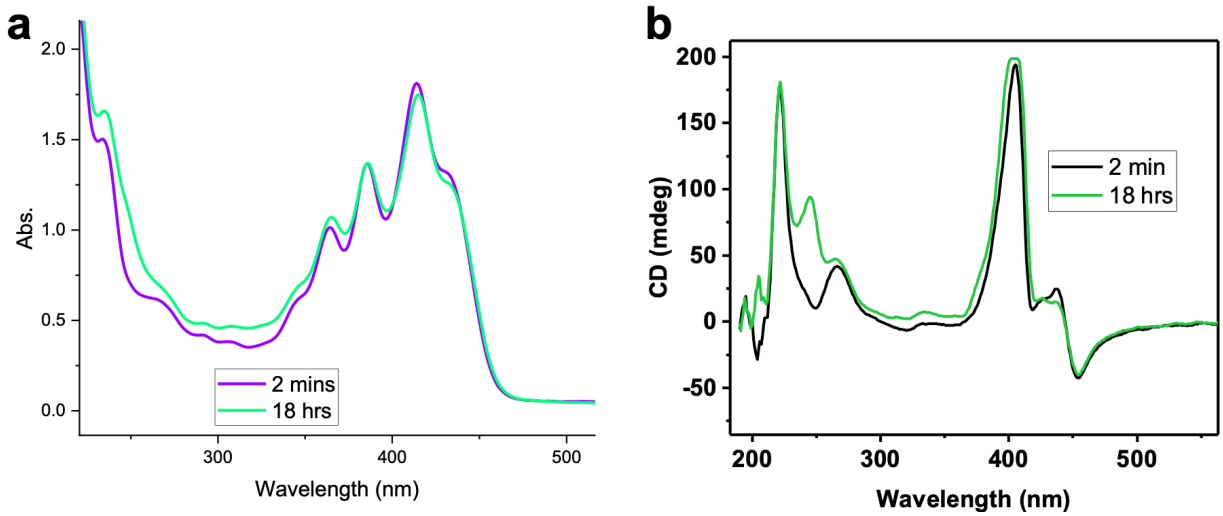

Figure S24. (a) CD and (b) UV-vis absorbance spectra of a sample of $\mathbf{1}_{NT}$ and $\mathbf{2}_{M}$ at pH 4.1 (2 mM, 1:1) and monitored for 18 h.

References

1. H. Shao, M. Gao, S. H. Kim, C. P. Jaroniec and J. R. Parquette, Aqueous Self-Assembly of L-Lysine-Based Amphiphiles into 1D n-Type Nanotubes *Chem. Eur. J.*, 2011, **17**, 12882-12885.
2. M. L. Mason, R. F. Lalisse, T. J. Finnegan, C. M. Hadad, D. A. Modarelli and J. R. Parquette, pH-Controlled Chiral Packing and Self-Assembly of a Coumarin Tetrapeptide *Langmuir*, 2019, **35**, 12460-12468.
3. H. Gaussier, H. Morency, M. C. Lavoie and M. Subirade, Replacement of trifluoroacetic acid with HCl in the hydrophobic purification steps of pediocin PA-1: a structural effect *Appl. Environ. Microbiol.*, 2002, **68**, 4803-4808.
4. A. Langlois and P. D. Harvey, Maple™-assisted calculations of the J-integral: a key parameter for the understanding of excited state energy transfer in porphyrins and other chromophores *J .Porphyr. Phthalocya.*, 2014, **18**, 666-674.